J. Mol. Biol. (1975) **94**, 425–440

Molecular Structure Determination by Electron Microscopy of Unstained Crystalline Specimens

P. N. T. Unwin and R. Henderson

Medical Research Council
Laboratory of Molecular Biology
Hills Road, Cambridge, England

(Received 15 November 1974)

The projected structures of two unstained periodic biological specimens, the purple membrane and catalase, have been determined by electron microscopy to resolutions of 7 Å and 9 Å, respectively. Glucose was used to facilitate their *in vacuo* preservation and extremely low electron doses were applied to avoid their destruction.

The information on which the projections are based was extracted from defocussed bright-field micrographs and electron diffraction patterns. Fourier analysis of the micrograph data provided the phases of the Fourier components of the structures; measurement of the electron diffraction patterns provided the amplitudes.

Large regions of the micrographs (3000 to 10,000 unit cells) were required for each analysis because of the inherently low image contrast ($<1\%$) and the statistical noise due to the low electron dose.

Our methods appear to be limited in resolution only by the performance of the microscope at the unusually low magnifications which were necessary. Resolutions close to 3 Å should ultimately be possible.

1. Introduction

The structure determination of unstained biological molecules by electron microscopy would be straightforward but for two principal factors. One is their high sensitivity to electron damage; typical proteins, for example, begin to disrupt at doses of the order of 1 electron/Å^2 (Stenn & Bahr, 1970), and such doses are far smaller than those used in routine observations. The other is the loss of three-dimensional order that generally takes place when the specimen's natural aqueous environment is replaced by the high vacuum of the microscope.

The high radiation sensitivity means that resolution in a "non-destructive" image of an isolated molecule is limited by electron noise to a figure of at least several tens of Ångstroms (Glaeser, 1973). A statistical barrier of this nature can be surmounted, however, if a highly ordered array of the molecules can be made, by utilizing the redundancy of information which is then present in the image (see e.g. McLachlan, 1958). A low dose image of this array will not display the projected structure of an *individual* molecule or unit cell directly; nevertheless, provided that the object is comprised of a large enough number of unit cells and that the periodicities are precisely maintained, all the information needed to reconstruct the "average" molecule

or unit cell will be available. There are a number of optical and computer methods for extracting such information (see e.g. Huxley & Klug, 1971).

The loss of order in the vacuum is, to some extent, prevented by conventional preparation methods in which the specimens are encased in negative stain, or fixed, embedded and sectioned; but these methods also restrict the information obtainable to comparatively gross features, such as the overall morphology of the specimen and the subunit structure. No information about the internal structure of the specimen is obtained. Elimination of such preparation procedures altogether by maintaining the specimen in a wet state with the aid of a hydration chamber (Parsons *et al.*, 1974) or by embedding it in ice (Taylor & Glaeser, 1974) in theory provides a more satisfactory solution; however, the technical problems associated with these methods may make high *image* resolutions difficult to achieve in practice.

The experiments we describe here using thin crystalline platelets of beef liver catalase suggest that a more profitable approach towards *in vacuo* preservation is to replace the aqueous medium by another liquid which has similar chemical and physical properties, but is non-volatile in addition. A number of sugars and related compounds have these properties and X-ray evidence (Unwin, unpublished results) indicates that they can be successfully substituted without greatly disturbing the order inherent in the native hydrated crystals, at least to a resolution of 3 to 4 Å. The second object we have used in these experiments, the purple membrane from *Halobacterium halobium*, is unusual in being almost unaffected by drying (Blaurock & Stoeckenius, 1971), but it also requires the presence of a similar fluid medium to minimize fragmentation or cracking of the membrane when it is allowed to dry down on the microscope grid.

This paper describes the determination of the projected structures of both catalase and the purple membrane to resolutions of 9 and 7 Å, respectively, by making use of the principles and methods of preservation that we have just outlined. Quantitative computer processing methods have been used to extract the data from the electron micrographs (DeRosier & Klug, 1968; Erickson & Klug, 1971) and this enables us to give objective assessments of the accuracy of the final structures.

The resolution limits in the present case are not set by poor specimen preservation or by radiation sensitivity, but mainly, we believe, by electron–optical factors that become important at relatively low magnifications. We are confident that our methods will be applicable to biological structure determination at resolutions close to the limit set ultimately by the microscope.

2. Experimental Technique

(a) *Specimen preparation*

Purple membranes were prepared according to the procedure of Oesterhelt & Stoeckenius (1974) from cultures of *Halobacterium halobium* R_1. Beef liver catalase crystals were prepared from a twice crystallized aqueous suspension (Sigma Chemical Co.) according to the NaCl dialysis procedure of Sumner & Dounce (1955). This procedure gave large numbers of platelets of a suitable thickness (400 to 600 Å as determined by shadowing from a known angle) for imaging and diffraction.

Solutions of either specimen were applied to carbon-coated grids and washed with a 1% solution, usually of glucose (but see also Results section (a)), before being allowed to dry—the technique being essentially the same as one would use for negative staining (e.g. Huxley & Zubay, 1960).

The character of the grids we used was different in the two cases. For the membranes

they were made to consist of a holey carbon film, coated with "gold islands", and overlaid with a thin carbon film; for the thicker catalase crystals they were made to consist simply of ~150 Å thick carbon film, coated very sparsely, but evenly, with the particles which are produced by evaporating gold in a vacuum of $\sim 10^{-1}$ torr. Micrographs of the purple membrane sheets were taken over holes in the thick carbon films. The "islands" and sparsely populated particles served as focussing aids.

(b) *Photographic materials*

For recording either images under normal dosage conditions, or electron diffraction patterns, we used Ilford Special Lantern Contrasty plates in conjunction with PQ Universal Developer (diluted 1+4). For recording under low dosage conditions we required a thin, fine-grained, emulsion having a low unit density exposure and a high detective quantum efficiency. We chose Kodak Electron Image plates for this purpose and these were developed strictly according to the manufacturers' instructions for maximum speed development (concentrated D19 developer, 12 min at 20°C). Since it was required to record both low and high dose images in pairs (see Theoretical Background section), the two types of plate were alternated in the camera box (and developed separately).

Optical density measurements from the Electron Image plates, interpreted with the aid of calibration charts supplied by Kodak, were the sources of electron dose estimates. Although such estimates may not be exact on an *absolute* scale (Matricardi *et al.*, 1972) they are reproducible and simple to obtain.

(c) *Electron microscopy*

Electron microscopy was carried out at 100 kV with a Philips EM301 using a narrow coherent illuminating beam, which was produced by having thin 25 μm (imaging) and 12 μm (diffraction) second condenser apertures and a strongly excited first condenser lens. The diameter of the illuminated area at the object plane, when recording the images, was about 5 μm. Electron diffraction patterns and conventional bright-field images were taken by standard techniques. No objective aperture was used.

For recording under low-dosage conditions we found it desirable to have a shutter above the specimen so that at any stage the entire grid under observation could be protected from irradiation. Our early attempts to provide an appropriate shutter action by making use of the deflection facilities were unsuccessful because it was found impossible with these to eliminate movement of the specimen image at high magnification during the first fraction of a second the illumination was applied. The shutter finally constructed consisted of a very simple mechanism which cut off or let through the electron beam by rapidly translating the first condenser aperture to either of two fixed positions; it did not appear to suffer from the above defect.

Further minor modifications to the microscope involved the mounting of a second, high-resolution phosphor (Levy–West Laboratories) viewing screen about 7 cm off the optical axis in the direction of the observer, and also a second set of ×15 binoculars with which to view it.

Before attempting to produce micrographs under low-dosage conditions, several steps other than the standard ones for high-resolution imaging had to be taken. Thus: (i) it was checked that an image feature placed on the optical axis (or a marked point on the central viewing screen) did not change its position significantly on varying the magnification over the range to be used (~500 to 40,000×); (ii) the deflection controls were preadjusted so that at the upper magnification the focussed beam, which illuminated the on-axis viewing screen when they were switched off, would illuminate the off-axis viewing screen when they were activated; (iii) two settings of the second condenser lens were noted, one being that required to give a focussed beam and the other being that required to give an expanded beam of an intensity such as to deliver the required low dose to the photographic plate in a 4 to 8 s exposure.

These preliminary steps having been carried out, a grid was scanned at a magnification of 500 to 1500×, using an illumination level ($\sim 5 \times 10^{-3}$ electrons/Å^2 per s in the plane of the object) just sufficient to detect specimen outlines (so that the dose delivered would be negligible in comparison with the dose needed for the photograph). On finding a

suitable area, it was placed accurately on the optical axis (or the marked point on the viewing screen) and immediately isolated from the electron beam by closing the shutter. Appropriate adjustments were then made at leisure.

These were such that the shutter would be re-opened with the magnification at the level required for taking the photograph, the beam focussed on the off-axis viewing screen, and the region of interest (to be illuminated subsequently) centred on the optical axis.

The final procedure was then simply to open the shutter, focus using the off-axis screen, close the shutter once again, switch off the deflection controls, expand the beam, move the photographic plate into position and expose by opening the shutter once more for a suitable length of time.

(d) *Data processing*

Optical diffraction was used to select regions in the low-dose micrographs which would be appropriate for further analysis and as a means for determining the contrast transfer conditions (see Theoretical Background section (a)); it further provided a valuable means of assessing the microscope's performance at various stages of the work. Otherwise we resorted to numerical methods of analysis involving densitometer measurement of the optical densities on the photographic plates and calculations by digital computer.

Intensity data had to be collected both from the electron diffraction patterns and from the low-dose micrographs. The very sharp diffraction spots (<40 μm in diameter) were scanned with a Joyce-Loebl mark IIIc microdensitometer, using a very small sampling aperture. Carefully selected regions in the low-dose micrographs were scanned with a Perkin-Elmer model 1010A automatic microdensitometer (with the help of Dr J. Pilkington of the Royal Greenwich Observatory, Herstmonceux, Sussex). The step and sampling aperture sizes in this case were 10 μm and 11×11 μm, respectively, and the areas recorded consisted of 2048×2048 arrays of optical density readings. The optical densities were measured at intervals of 0·005, which is sufficiently accurate to record the variation due to statistical noise without significant error.

To establish the reciprocal space co-ordinates of a few of the stronger reflections in the Fourier transforms of each array, and hence the reciprocal lattice vectors, we initially processed a 1024×1024 region from the array on an IBM 370/165 computer, using a fast Fourier transform program written by L. Amos and L. Ten Eyck. Subsequently, to calculate the full transforms at the reciprocal space positions of all of the reflections, each 2048×2048 array was processed using the IBM 370/165 for carrying out the transform in one dimension and a PDP11/10 for carrying it out (on selected regions only) in the other. (The use of separate computers was a convenience rather than a necessity.) The final PDP11 output was in the form of 9×9 grids of amplitudes and phases, centred over each of the calculated positions of the reflections. An example of the form of the final amplitude output is given in Fig. 3.

3. Theoretical Background

We planned to combine data from bright-field images and electron diffraction patterns to determine the projected structures of the two specimens. Basically, the method proposed was to filter out statistical noise in Fourier transforms of selected low-dose micrographs by utilizing the phases at the reciprocal lattice points in the transforms, and to combine these phases with the amplitudes established by measurement of the intensities in the electron diffraction patterns. The electron diffraction intensities were to be used because they provide more accurate amplitude data than the image transforms (see Results section (c)). The resulting Fourier synthesis should give an undistorted map of the structure.

The validity of the maps obtained in this way depends largely on how faithfully the bright-field image records the projected structure; the general usefulness of the method depends to a great extent on the area of micrograph that needs to be

processed to generate the necessary information. These aspects are of primary importance and it is appropriate now to discuss them in some detail.

(a) *Bright-field imaging of unstained periodic objects*

Diffraction of electrons by a periodic object is caused by periodic modulations in the potential field distribution associated with its constituent atoms. With unstained material (immersed in a liquid of similar density), these modulations are small, since the contributions due to the various small groups of like atoms placed more or less irregularly within the unit cell are similar and tend to cancel out. Therefore, diffraction is very weak in comparison, say, with that from thin, negatively stained biological specimens.

In order to describe this interaction, it is convenient to represent the incident electron beam by a coherent plane wave of amplitude unity. This, on passing through the potential field of the object is modified by a transmission function, $\exp(i\sigma\phi(x, y))$, where $\phi(x, y) = \int_{-\infty}^{\infty} \phi'(x, y, z)dz$ is the projection in the beam direction of the three-dimensional potential distribution, $\phi'(x, y, z)$, in the object, and $\sigma = \pi/\lambda E$, E being the accelerating potential. The wave function immediately behind the object is therefore:

$$\begin{aligned} \psi(x_0, y_0) &= \exp(i\sigma\phi(x_0, y_0)), \\ &\simeq 1 + i\sigma\phi(x_0, y_0), \end{aligned} \tag{1}$$

since the effect of the potential field on the incident electrons is small (weak phase object approximation).

A further term is sometimes included in equation (1) to account for attenuation of the coherent incident wave by, for example, inelastic scattering. This "amplitude" component is, however, weak in comparison with the phase component given above, and since its influence is undetectable in bright-field images of carbon films (Thon, 1971) it is reasonable to neglect it in a discussion of bright-field images of unstained specimens (see, however, footnote on p. 434).

The wave function at the diffraction plane is the Fourier transform of $\psi(x_0, y_0)$, multiplied by a phase factor, $\exp(i\chi)$, i.e.:

$$\Psi(h, k) = F(\psi(x_0, y_0))\exp(i\chi), \tag{2}$$

the integer variables h and k being used to indicate that we are dealing with a periodic object which produces discrete reflections on a reciprocal lattice. The factor, $\exp(i\chi)$, accounts for the modification of the phases of the various reflections as a result of defocussing and spherical aberration. The magnitude of this phase shift is given by:

$$\chi = 2\pi\lambda^{-1}\,(\delta f\theta^2/2 - C_s\theta^4/4), \tag{3}$$

where δf is the degree of underfocus, C_s is the spherical aberration coefficient and θ is the scattering angle.

Equation (2), using the approximation in equation (1), becomes:

$$\Psi(h, k) = \delta(0, 0) - \sigma\Phi(h, k)\sin\chi + i\sigma\Phi(h, k)\cos\chi, \tag{4}$$

where $\delta(0, 0)$ is a delta function representing the unscattered electron beam at the origin and $\Phi(h, k)$ is the Fourier transform of $\phi(x_0, y_0)$. The Fourier transform of $\Psi(h, k)$ gives the wave function, $\psi(x_i, y_i)$, at the image plane. However, since it is the intensity distribution, $|\psi(x_i, y_i)|^2$, that is recorded and since $\sigma\Phi(h, k) \ll \delta(0, 0)$, it is

clear from equation (4) that the imaginary part of $\Psi(h, k)$ contributes to the image squared terms only in quantities which are small. Therefore, in considering the Fourier terms which make up the image, only the real part of equation (4) is relevant. Thus the Fourier transform of the intensity distribution in the image is proportional to:

$$\delta(0, 0) - 2\sigma\Phi(h, k)\sin\chi.$$

$-2\sin\chi$, known as the *phase contrast transfer function*, is a term which modulates the amplitudes of $\Phi(h, k)$ and the signs of its phases. A plot of this function for a typical case is given in Figure 2(c). Its significance is of course that it relates the Fourier transform of the object to the Fourier transform of its image, and we have made use of this direct relation to establish the phases of the reflections originating from our specimens.

This approach, which was implicit in discussions by Hanszen & Morgenstern (1965) and by Hoppe (1970), has been shown to be applicable to thin, negatively stained specimens by Erickson & Klug (1970,1971).

The approach is valid, at least in the absence of effects due to curvature of the Ewald sphere (see Results section (a)), if (i) the second and higher-order terms in the expansion of $\exp(i\sigma\phi(x, y))$ are too small to introduce appreciable error, and (ii) the specimens are sufficiently thin that Fresnel diffraction effects (Cowley & Moodie, 1957) may be neglected.

The former source of error can be evaluated roughly from observed figures for $|F_{\max}|^2$, the intensity of the strongest reflection in the electron diffraction pattern relative to the intensity of the unscattered beam. For either material under investigation (see Results section (a)), $|F_{\max}|^2 < 5\times10^{-5}$†. Since the *phase* modulation of the incident wave by a Fourier component of the potential distribution in the object plane is directly related to its *amplitude* in the diffraction plane, this means that the phase modulations responsible for the strongest reflections are the order of 10^{-2} rad or less (and the contrast associated with them in the image, less than 1%). The greatest contribution from the second and higher-order terms arising from one Fourier component is therefore ~0·5% of the first-order term, i.e. certainly small enough to be neglected.

The effect of finite object thickness is to multiply the amplitude distribution in the diffraction plane by an additional phase factor, $\exp(i\pi Z\theta^2/2\lambda)$ (Cowley & Moodie, 1957), where Z is the specimen thickness. Clearly the higher the scattering angle, θ, the more significant does this source of error become. For the image resolutions we obtain however, the maximum value of the phase shift from this effect is only $\pi/6$ for the thicker specimen and $\pi/60$ for the thin one. These are still small shifts and consequently we do not expect the effects of finite object thickness to be very important.

(b) *Estimation of the required number of unit cells*

An estimate of the number of unit cells needed to provide sufficient information is useful for demonstrating the theoretical feasibility of our method. It is also important in practice that the required number of unit cells should fit easily onto a normal photographic plate.

† To appreciate the smallness of this figure it should be compared to the equivalent figure of 0·06 obtained by Gerchberg (1972), from the same catalase crystals, negatively stained.

A simple way of estimating this number is to divide the object into elements having the same projected area as a single unit cell, and assume each such element to be irradiated, on average, by aN electrons (N electrons/Å^2 incident on unit cell area, a Å^2). One then represents the electrons incident on n of the unit cells by a random array of delta functions. Now it is easily shown that in the Fourier transform of such an array, the amplitude at any general point is, on average, $(naN)^{\frac{1}{2}}$, compared to naN at the origin. These quantities would apply to the Fourier transform of the image intensity distribution, but for the fact that only a fraction (f) of the electrons incident on the object are actually detected on the photographic plate. Allowing for this, the "noise" in the Fourier transform of n unit cells in the image, expressed as a fraction of the amplitude at the origin, is $(fnaN)^{\frac{1}{2}}/(fnaN) = (fnaN)^{-\frac{1}{2}}$.

The strength of the weakest "signal" to be detected in the Fourier transform of the image intensity distribution, scaled in the same way, is $2|F_{\min}|$ (i.e. twice the amplitude of the weakest relevant reflection in the *electron* diffraction pattern divided by the amplitude at the origin). If N' is taken as the maximum dose over which the periodic detail in the specimen remains intact (see also Results, section (a)), we have then: $2|F_{\min}| > (fnaN')^{-\frac{1}{2}}$, or $2|F_{\min}| = k(fnaN')^{-\frac{1}{2}}$ for a detectable signal to be obtained on Fourier transforming n unit cells. Alternatively, the minimum number of unit cells required to be present in the image is:

$$n = k^2/4faN'|F_{\min}|^2. \tag{5}$$

The effect of noise from the substrate is not accounted for in this equation. However, provided that the actual dose given does not greatly exceed N' and that the substrate is not significantly more strongly scattering (i.e. thicker) than the specimen, it is likely to be small in comparison with noise of a statistical nature.

Since the "signal" in the Fourier transform of the image consists of discrete, regularly spaced peaks whose positions can be decided on with precision, the factor, k, in equation (5) (i.e. the ratio of the weakest peak to r.m.s. noise) can be quite small. Experimental measurements (Results, section (c)) show that a value of 1 would be satisfactory for perfect contrast transfer, but more generally we would expect a value of, say, 2 to be appropriate. The magnitude of f depends on the thickness of the specimen (since this determines the number of electrons which reach the image) and the detective quantum efficiency of the photographic plate; we estimate f to be about $\frac{1}{2}$ for purple membrane and $\frac{1}{4}$ for catalase. If we further anticipate our electron diffraction results (Results, section (a)) and put $N' = 0{\cdot}5$ electrons/Å^2, $|F_{\min}|^2 = 10^{-6}$, we obtain a required minimum number of about 1200 unit cells for purple membrane (unit cell area ~3300 Å^2) and 700 unit cells for catalase (unit cell area ~12,000 Å^2).

These numbers of unit cells can easily be accommodated on the normal photographic plate without having to resort to unduly low magnifications where high image resolution would be difficult to attain. Therefore, it should be possible to obtain single bright-field electron micrographs of such objects which contain all the required structural information. In practice, because of missing information at the zeros of the contrast transfer function, at least two would be required.

Finally, we draw attention to the fact that in contrast to the related expression for visualizing isolated molecules (e.g. Glaeser, 1973) equation (5) says nothing about resolution. A resolution limitation is however implied, since $|F_{\min}|$ is, in general, the highest resolution reflection in the object's electron diffraction pattern. Of course, it might not be possible to attain the resolution predicted by equation (5) if the specimen

is coherently ordered to a resolution which is greater than that of which the microscope is capable. It will become evident below that this is the case with our specimens.

4. Results

(a) *Electron diffraction*

Electron diffraction patterns (Plates I and II) demonstrate that crystalline order is preserved out to at least 3·5 Å in both the purple membrane sheets and the catalase platelets immersed in glucose. This resolution is close to that we obtain by X-ray diffraction and therefore refers to the inherent degree of order in the specimens.

Electron diffraction patterns of catalase having *low-angle* intensity distributions somewhat different from those shown in Plate I may be obtained by immersing the crystals in media composed of sucrose, ribose, inositol and other small hydrophilic molecules, which form reasonably stable non-volatile fluids. Such a variation in the low-angle intensity distribution is to be expected with media having slightly different densities, close to that of the protein (see e.g. Bragg & Perutz, 1952; Harrison, 1969). The high-angle intensities on the other hand are almost identical in the different media. This latter observation strongly suggests that the structure of the native hydrated protein is not greatly altered when the aqueous solution is replaced. Presumably, therefore, the properties of these sugars and related compounds are sufficiently close to those of water that they interact with the protein in a similar way.

The relative intensities of the reflections in the diffraction patterns shown in Plates I and II were sensitive, by differing degrees, to (i) the deviation of the normal of the plane of the specimen from the direction of the incident beam and (ii) the electron dose. The first factor is only of consequence with the catalase crystals and is due to the combined effect of their thickness (meaning that the reflections only extend a relatively short distance in reciprocal space) and the curvature of the Ewald sphere. It is easy to show that the 3·5 Å resolution reflections in the catalase pattern will only just touch the Ewald sphere when the crystals are exactly oriented. This means that deviations as little as $\frac{1}{2}^\circ$ are sufficient to disturb the symmetry of the intensity distribution in the high-angle region quite noticeably. The effect will of course be evident in the image and needs to be minimal in the micrographs from which the projections are to be calculated, since it may lead to detail which is not representative of the detail that a true projection down the *c*-axis would show. Particular care therefore has to be taken with catalase in selecting micrographs which are appropriate, but this does not become a serious problem in practice until resolutions beyond our present 9 Å.

The behaviour of the two materials as a function of electron dose is illustrated in Figure 1. With purple membrane, the reflections decay exponentially (to a good approximation), at rates which are similar, although tending to be slightly more rapid at higher resolutions. With catalase on the other hand, while the higher resolution reflections tend to decay exponentially and at similar rates, the lower resolution reflections alter in a variable manner, a few actually increasing in intensity during the initial period of exposure.

Comparing the two sets of dose-response curves, it is interesting to note a good correspondence between the two materials in the decay rates of the highest resolution reflections. Since fading of diffraction patterns is due to loss of long-range order, the

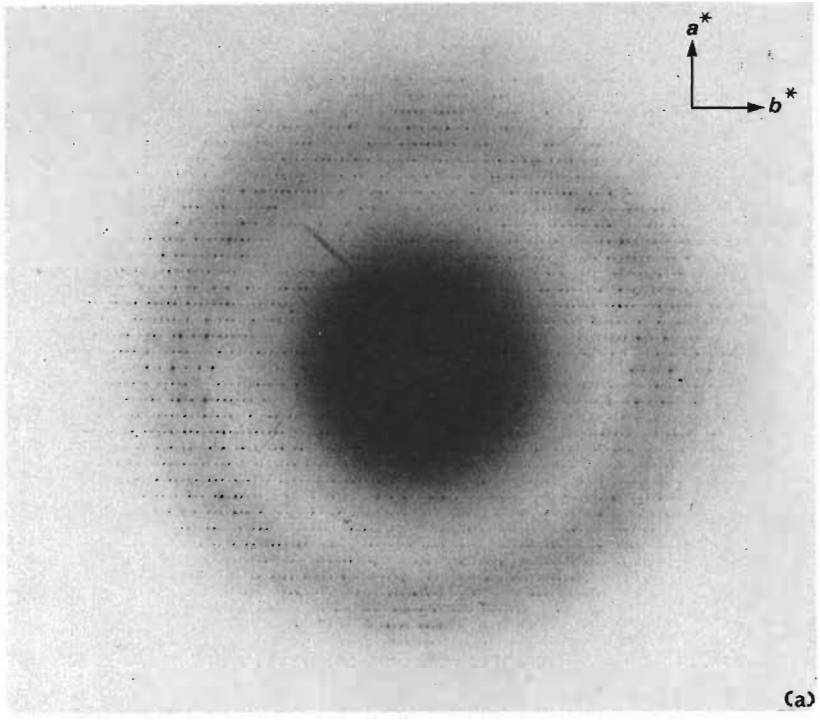

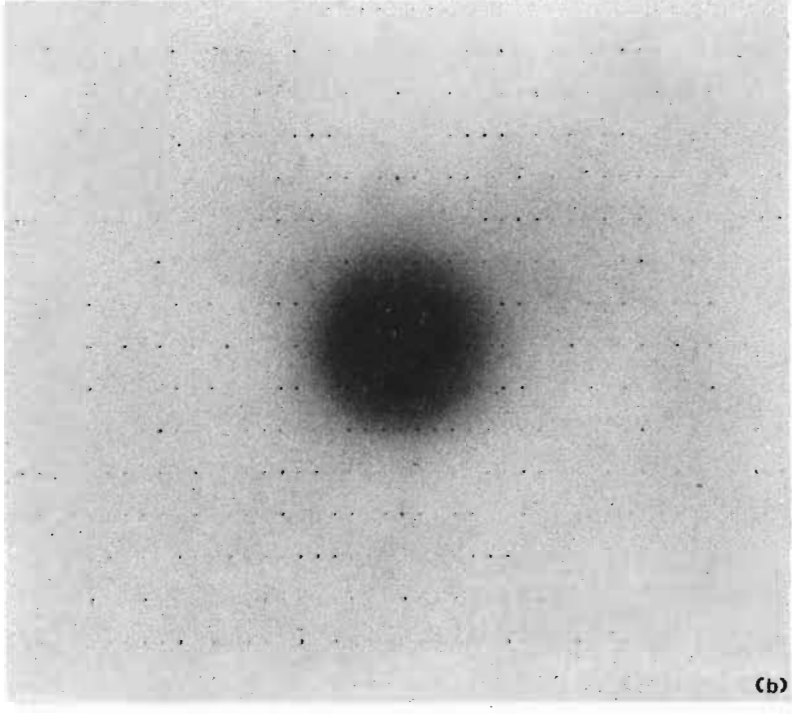

PLATE I. Typical electron diffraction patterns from nearly exactly oriented (see text) catalase crystals immersed in glucose; (a) high-angle and (b) low-angle pattern. The two patterns are shown separately since low-angle inelastic scattering makes it impossible to reproduce both in one picture. The fact that reflections from upper layer planes are not present in (a), means that the resolution limit does not extend much beyond 3·5 Å. Scales: (a) 1 cm: 0·068 $Å^{-1}$; (b) 1 cm: 0·026 $Å^{-1}$.

[*facing p. 432*

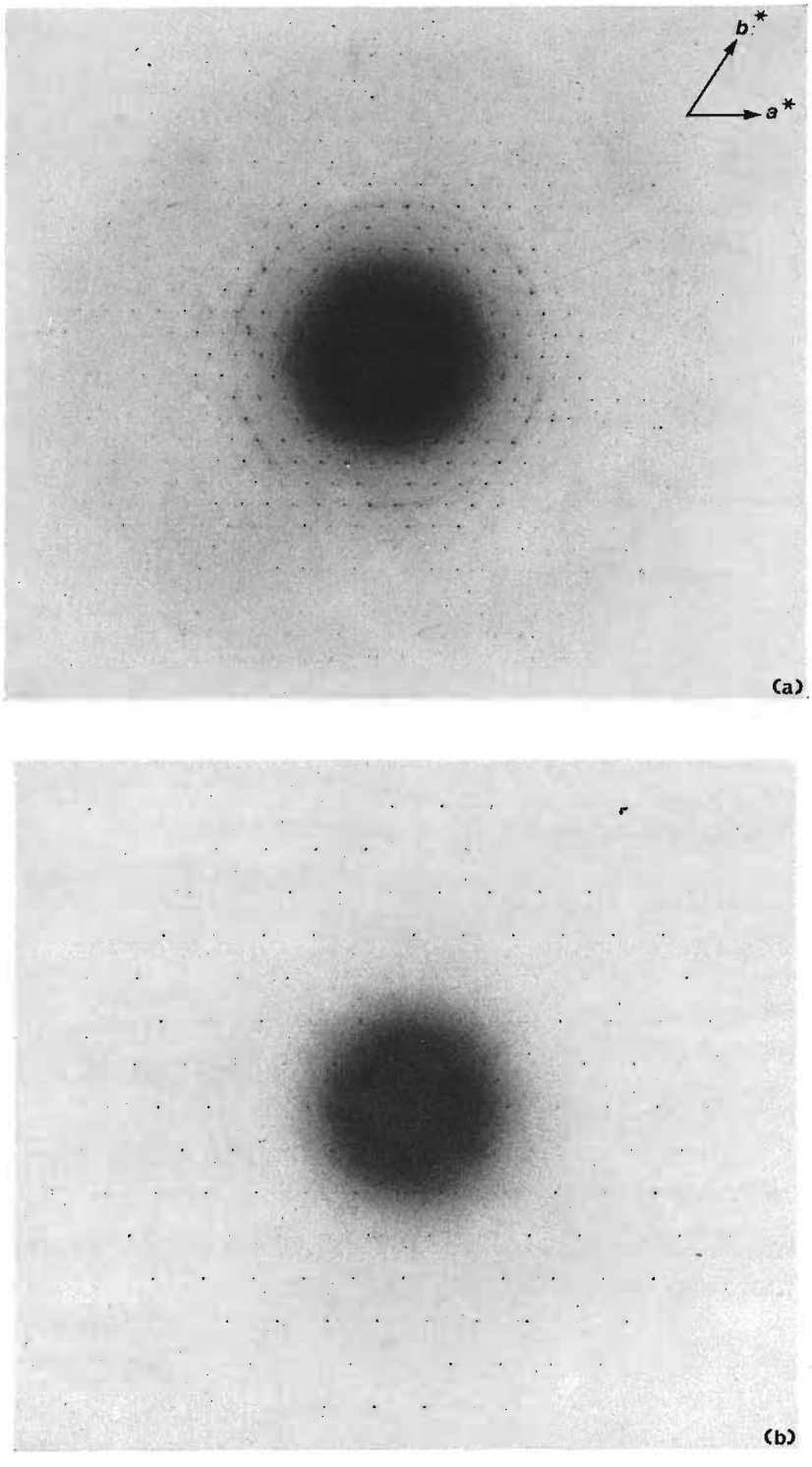

PLATE II. Typical electron diffraction patterns from the purple membrane; (a) high-angle and (b) low-angle pattern. They are from reconstituted membrane (Henderson, unpublished results), not the native one on which the micrographs are based. The distribution of intensities is the same in either case, but the reconstituted membrane has a better signal to noise ratio since it contains a much greater number of unit cells. Scales: (a) 1 cm: 0·056 $Å^{-1}$; (b) 1 cm: 0·028 $Å^{-1}$.

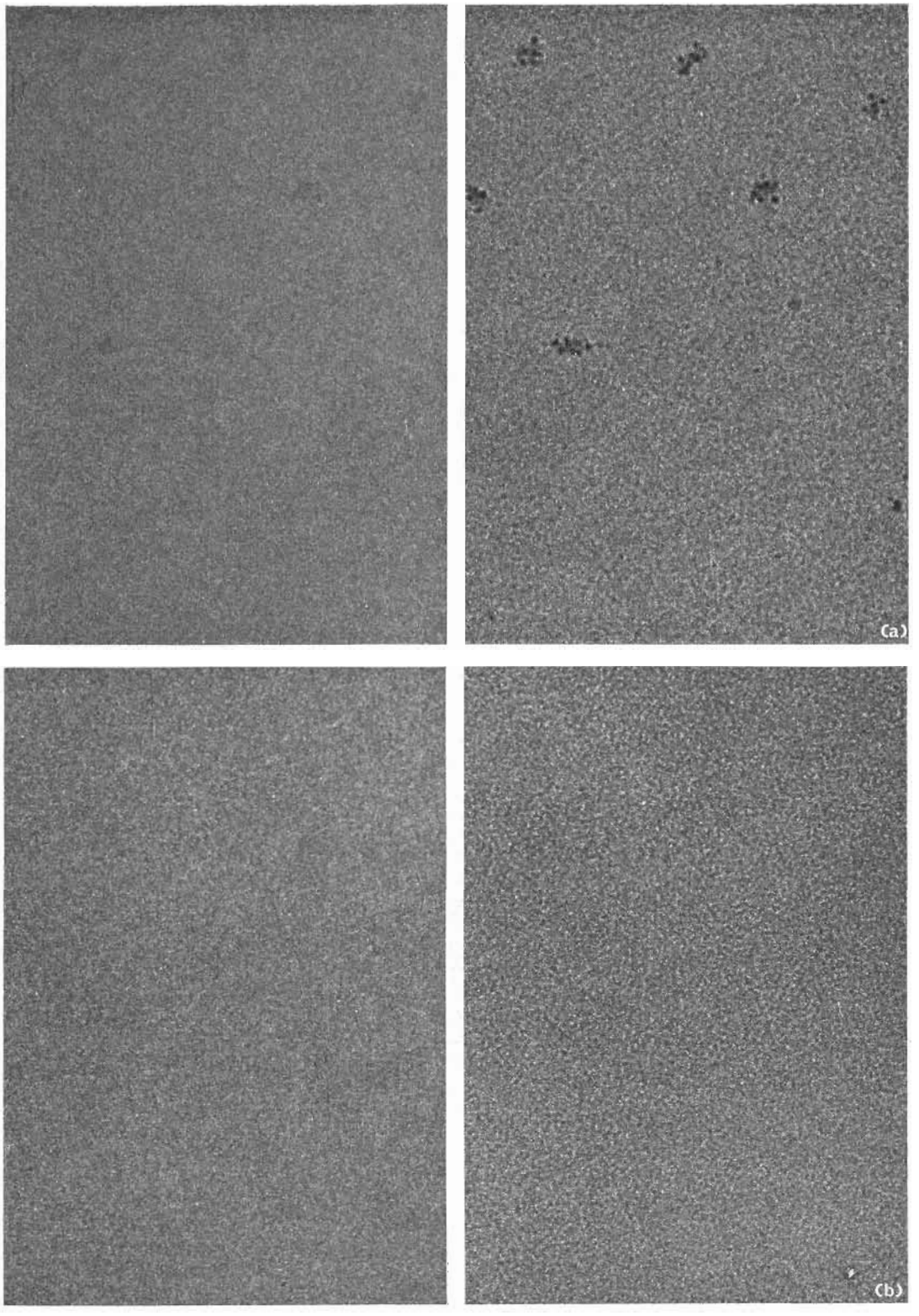

PLATE III. Typical low-dose and high-dose (longer exposure), bright-field micrographs of the same regions of (a) catalase and (b) purple membrane. The gold particles, used as focussing aids, can be seen in (a).

The two types of specimen are about equally sensitive to radiation damage and in both cases only the low-dose pictures contain significant detail about their structure; however, because of the low signal to noise ratio present in the low-dose pictures, such detail cannot be detected by eye. The high-dose pictures contain information on the contrast transfer conditions (see also Plates IV and V). Magnification: all at 500,000×.

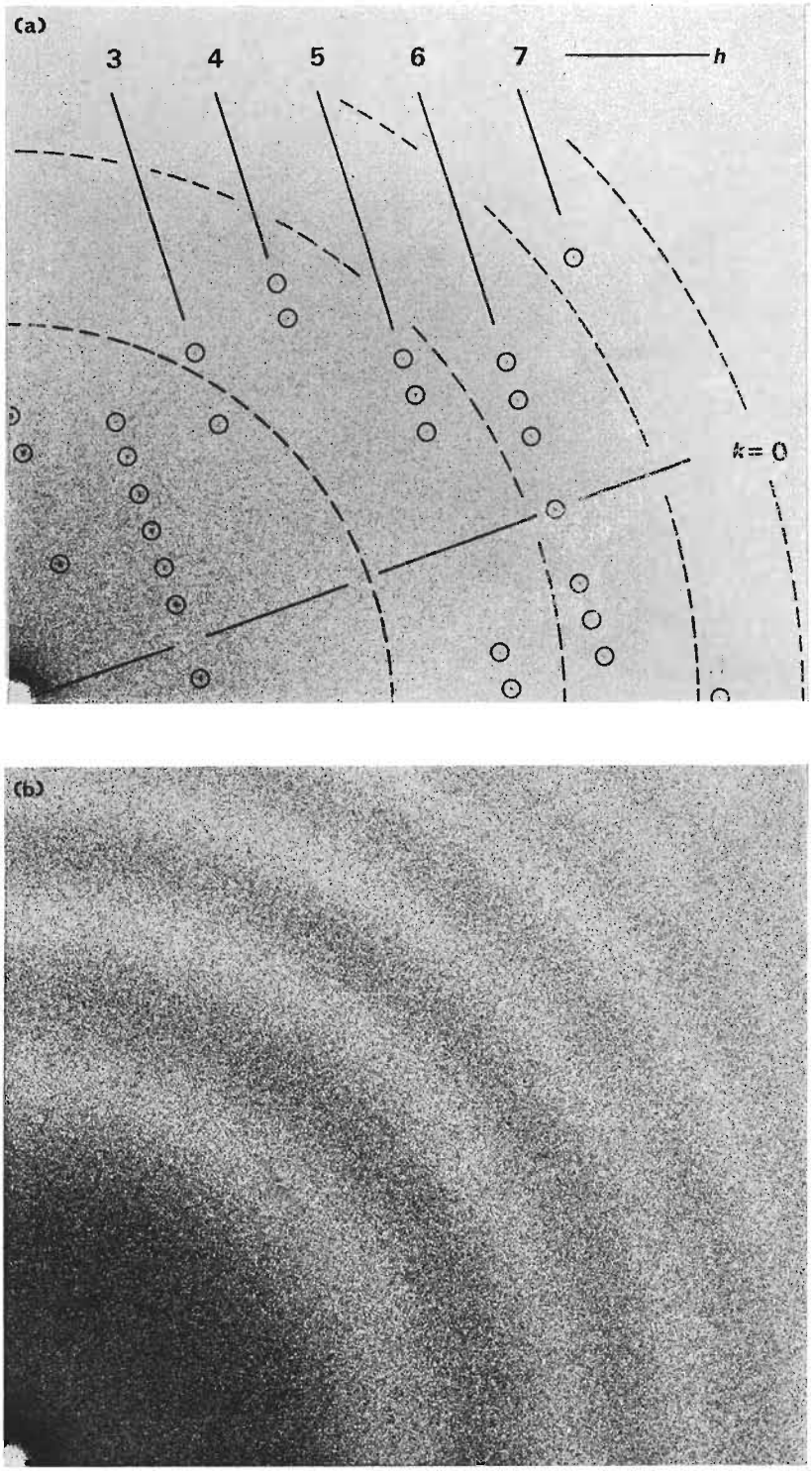

PLATE IV. Optical transform quadrants of the catalase micrographs containing the regions shown in Plate III; (a) of the low-dose micrograph, (b) of the high-dose micrograph. Peaks on the lattice corresponding to that in the electron diffraction pattern are evident in (a), their intensities being modulated according to the intensity distribution in (b).

Only the stronger peaks (circled) are readily observed in (a) (also in Plate V(a)) but this is partly because they are extremely sharp and hence difficult to reproduce photographically (the computed transforms, e.g. Fig. 3, indicate that their diameter should be less than 100 μm on the scale given). The positions of the minima in (b) are indicated by broken lines in (a). Scale: 1 cm: 0·011 Å^{-1}.

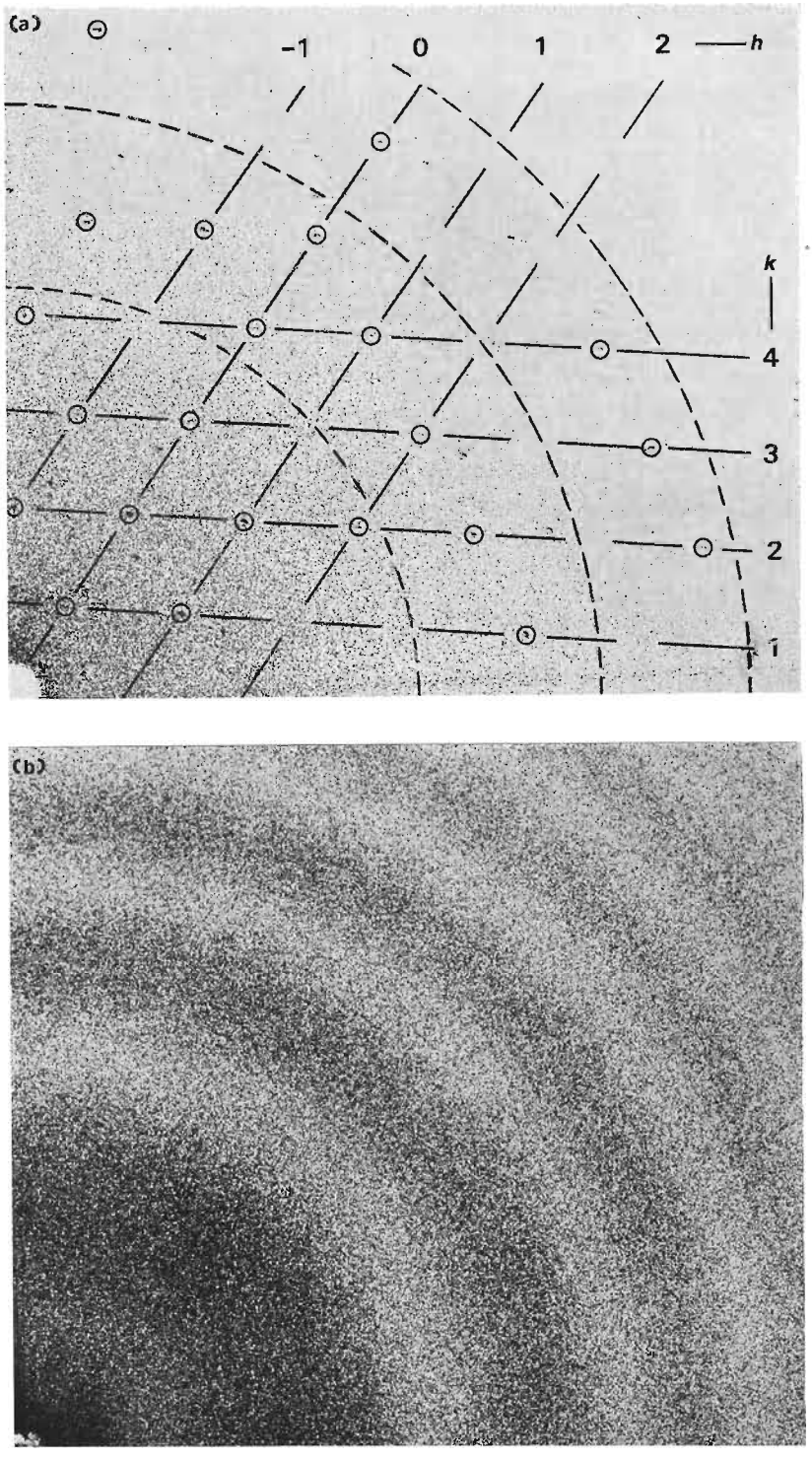

PLATE V. Optical transform quadrants of the purple membrane micrographs containing the regions shown in Plate III; (a) of the low-dose micrograph, (b) of the high-dose micrograph. There are two membranes in different orientations contributing to the peaks in (a); the lattice formed by one of them is indicated. Scale: 1 cm: 0·012 $Å^{-1}$.

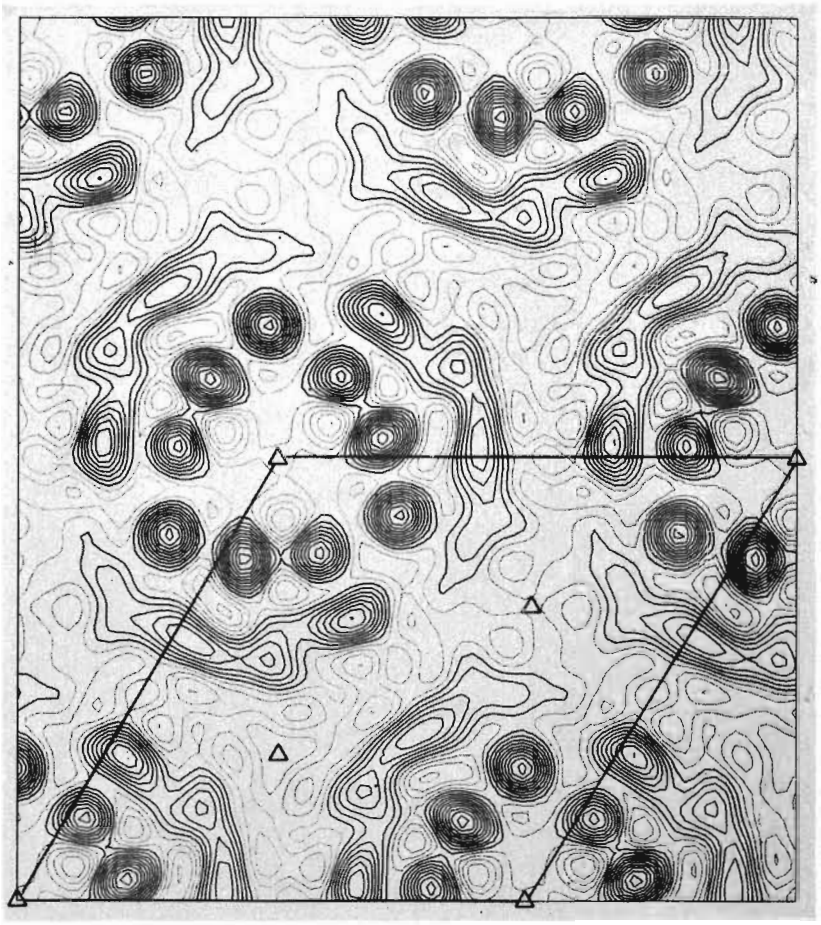

(a)

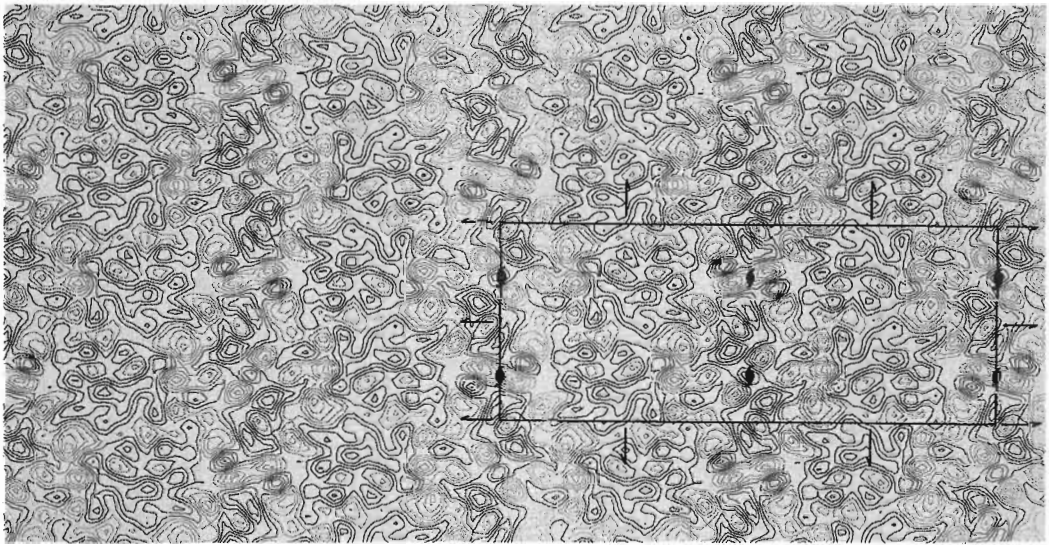

(b)

PLATE VI. Contour maps of the projected structures of (a) the purple membrane at 7 Å resolution and (b) catalase at 9 Å resolution, calculated according to the methods described in the text. The $F(0, 0)$ term was excluded from the syntheses. Positive contours are indicated by thicker lines; the positive peaks are due to high concentrations of scattering matter (such as dense regions in the protein). The unit cell dimensions shown in (a) are 62 Å × 62 Å and in (b) 69 Å × 173·5 Å.

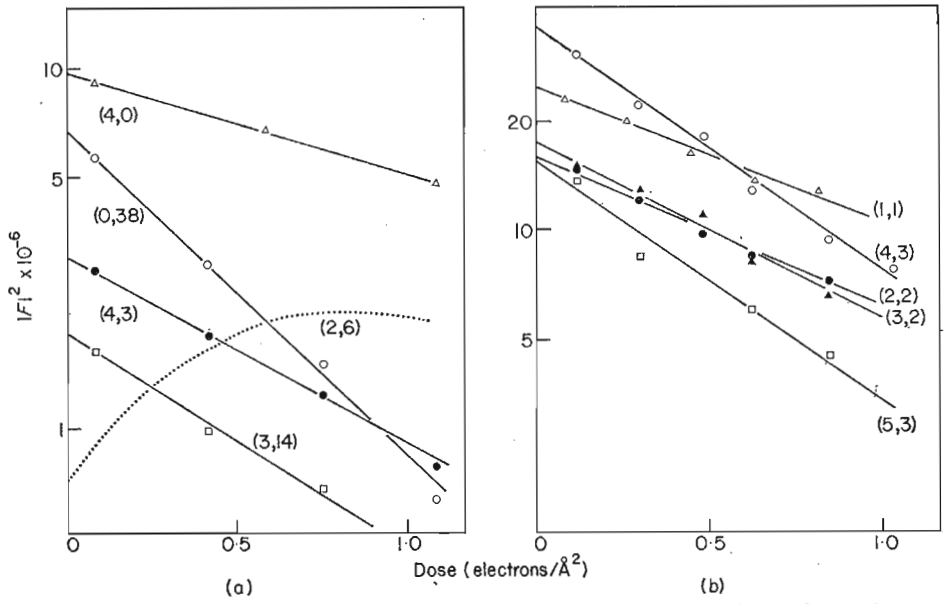

FIG. 1. The intensities (on a logarithmic scale) of some typical reflections in (a) the catalase and (b) the purple membrane electron diffraction pattern, plotted as a function of electron dose. The data for (a) were taken from "exactly oriented" single crystals (where the symmetry and Friedel-related reflections all have equal intensities), the dotted curve referring to one of the few reflections which actually increase in intensity during the initial exposure period. (Such reflections are at variance with the more typical behaviour, over the dose range shown, of exponential decay.) The data for (b) were taken from the "ring" diffraction patterns produced by a large number of native membranes several layers thick, so that the intensity of the (4, 3) ring is contributed by both the stronger (4, 3) and the weaker (3, 4) lattice reflection, and so on.

The intensities are scaled relative to unit intensity for the unscattered beam (where the area contributing to the diffraction pattern is smaller than that occupied by the specimen and there is only one specimen present). The absolute figures are more approximate in the case of catalase, where there is some variation in thickness from one crystal to the next.

correspondence probably reflects similarities in the strengths of the bonds stabilizing the two assemblies.

It is the highest decay rates that determine the characteristic dose, N', and hence the length of exposure required for the micrograph. Since the reflections should retain a good proportion of their original intensity over the total exposure period, and since the highest decay rates are approximately exponential, it seems reasonable to define the characteristic dose as that dose over which the *fastest fading peaks* have fallen to $1/e$ of their original intensity. This gives $N' = 0{\cdot}5$ electrons/Å^2 for both specimens.

The strongest reflections are the (4, 3) in the purple membrane diffraction pattern and the (0, 4) in the catalase diffraction pattern. The intensities of these reflections, as fractions of the unscattered beam are $2{\cdot}5\times10^{-5}$ and 4×10^{-5}. 90% of the reflections from either structure are greater than 10^{-6}, i.e. 1/25 of the strongest intensity in the purple membrane case and 1/40 of the strongest intensity in the catalase case. Our aim is to include in the structure analysis all reflections above this limit. The exclusion of the remaining 10% of extremely weak reflections will have an insignificant effect on the final result. It is the strength of the weaker reflections which are to be included which determines the number of unit cells to be processed (see Theoretical Background section (b)).

(b) *Imaging*

The photographic factors which influence the choice of magnification for a low-dose image are (i) the resolution of the emulsion and (ii) the fog level. Our measurements on electron image plates gave figures of ~10 μm and 0·03 optical density units for (i) and (ii), respectively, the magnitude of the former figure being a consequence of spread of electrons in the photographic emulsion (Hamilton & Marchant, 1967) rather than grain size. On this basis, the lower limit in magnification for, say, a 5 Å map is 20,000×. The upper limit is encountered when the optical density recorded on the plate produced by the dose required to disrupt the specimen (N') approaches the fog level. Allowing for attenuation of the incident beam by the specimen and assuming a unit density exposure of 0·46 electrons/μm^2 (estimated from data supplied by Kodak), we obtain an upper limit of about 40,000× for purple membrane, and a somewhat lower figure for catalase, where the attenuation is greater.

The latter magnifications fortunately coincide with the practical requirement of having the size of the areas that need to be processed a fair amount smaller than the plate size; we accordingly chose magnifications of 40,000× and 33,000× for purple membrane and catalase, respectively, and exposures which gave optical density readings of about 0·1. (These exposures correspond to doses a little greater than N'.)

The typical low dose and high dose (longer exposure) micrographs we obtained for each of the two specimens are illustrated in Plate III. It is not possible to detect by eye any periodicities in the low-dose pictures,† although their presence is of course obvious from their Fourier (or optical) transforms (see below). The repeating structure rapidly disappears under irradiation and the second micrographs from each of the specimens show little or no evidence for it. These micrographs, being exposed by a dose approximately ten times that of the low-dose micrographs, are however less statistically noisy and therefore display the usual "out of focus" granular phase detail distinctly.

(c) *Image analysis*

Computed and optical transforms of the low-dose electron micrographs (Fig. 3 and Plates III(a) and IV(a)) display discrete peaks on well-defined lattices, identifiable of course with those in the electron diffraction patterns; optical transforms of the high-dose micrographs (Plates III(b) and IV(b)) display concentric rings of intensity (Thon, 1966) deriving from the contrast transfer conditions prevailing. The computed transforms of the low-dose micrographs provided the phases at the lattice points of the transform of the specimen *image*. The optical transforms of the high-dose micrographs were then used to decide which of these image phases needed no modification and which required adjustment by 180° to produce the correct phases for the *object*‡.

The amplitudes of the structure factors were obtained by measurement of intensities

† With catalase the low resolution periodicities can be seen in over-exposed, low dose, micrographs. This is because they are associated with low-resolution diffraction peaks, some of which are relatively insensitive to electron dose.

‡ All the micrographs analysed were of under-, rather than over-focussed images. Therefore, in every case, the regions up to and including the first ring in the optical transforms, and every alternate ring thereafter, are associated with phase changes of 180° (cf. Fig. 2(c)).

Note that in the under-focussed image any small, low-frequency contribution due to amplitude contrast adds to the phase-contrast effect (see Erickson & Klug, 1970). The under-focussed image therefore avoids any ambiguity of sign in the low-angle region, which could arise in an over-focussed image with some amplitude contrast present.

in the electron diffraction patterns. We believe it is better to use the electron diffraction pattern rather than the Fourier transform of the image for this purpose because the electron diffraction pattern is insensitive to effects associated with the contrast transfer function and gives all the intensities on the same scale.

The ratios of the amplitudes computed from individual low-dose micrographs to the amplitudes from the electron diffraction patterns, when plotted against spatial frequency, form curves showing a series of well-defined maxima and minima (Fig. 2). The positions of these maxima and minima can be identified almost exactly with those in the optical transforms of the corresponding high-dose micrographs and are consistent with the theoretical contrast transfer functions calculated after estimating, from the high-dose micrograph, the degree of under-focus (see Fig. 2). We can thus confirm

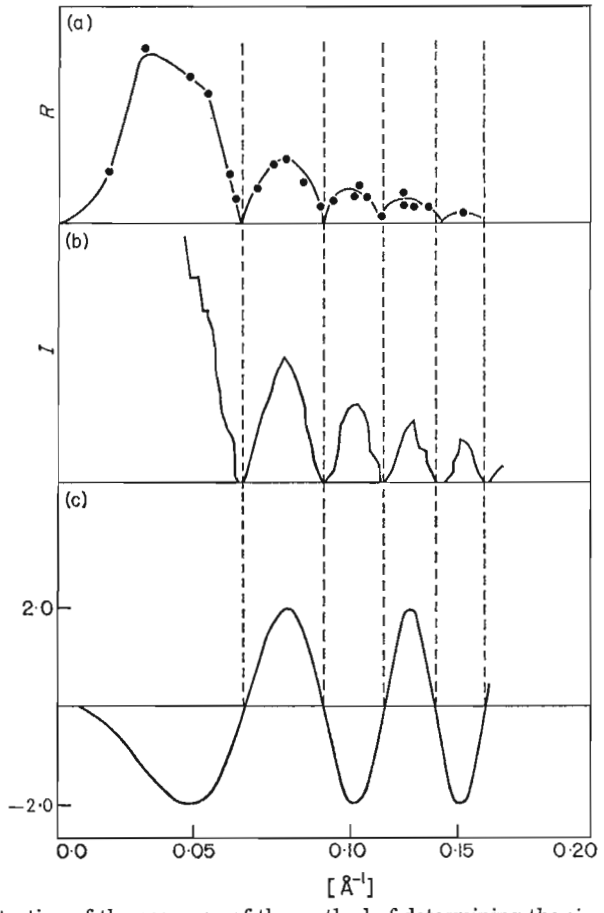

FIG. 2. Demonstration of the accuracy of the method of determining the signs of the phases by using information from a second micrograph. (a) The structure factor amplitudes calculated from a low-dose micrograph of the purple membrane as ratios (R) of their electron diffraction values, plotted against spatial frequency; they form a curve consisting of a series of maxima and minima. (b) The background-corrected intensity (I) across the optical transform of the corresponding high-dose micrograph; the positions of its maxima and minima match up almost exactly with those in (a). (c) The phase contrast transfer function appropriate to (b) (under-focus = 5750 Å; spherical aberration coefficient = 1·6 mm), illustrating how the sign assignments are made.

In principle, and as is evident from (a), a second micrograph is not strictly necessary for determining the signs of the phases. However, in practice, for a reliable determination, it is more or less essential.

that the focus does not change significantly between the low and the high-dose exposures and hence that the method involving pairs of micrographs for correcting the structure factor phases is accurate.

Figure 3 shows some typical computed matrices of amplitudes obtained by Fourier transformation of the 2048×2048 optical density arrays in the low-dose micrographs. On establishing the exact positions of a number of the strong high-resolution peaks in the lattices we were able to calculate the reciprocal space co-ordinates of all peaks in the transform with a precision of better than 1/5 of the grid spacing in X and Y, and hence obtain objective measurements of phase at each reciprocal lattice point. However, we collected data only from those peaks whose amplitudes were equal to or higher than the r.m.s. noise level ($k = 1$ in equation (5)). Statistical considerations indicate that peaks which are appreciably weaker than the noise level will have a mean error in phase of between 45° and 90° (90° being the figure for random phases). Even lower ratios of signal to noise than those used could nevertheless be accepted if one were to include data from more micrographs and extend the averaging procedure that is outlined below.

We investigated the accuracy of the phase determinations by taking account of the symmetry existing in the two structures.

In the catalase diffraction pattern, systematic absences along the $(h, 0)$ and $(0, k)$ lattice lines point to the presence of two mutually orthogonal 2_1 screw axes. Therefore the observed c-axis projection is centrosymmetric. (A related unpublished study of the same catalase crystals and single layers, negatively stained, indicates further that the crystals are orthorhombic with space group symmetry $P2_12_12_1$.) Ideally then, all the phases in the Fourier transform of the catalase micrograph, with an appropriately adjusted phase origin, should be 0° or 180°. In addition, the signs, s, of symmetry related reflections in the two independently recorded quadrants are simply related ($s(h, k) = (-1)^{h+k}\, s(h, -k)$).

The purple membrane is composed of protein and lipid molecules which are arranged as a layer one unit cell thick in space group $P3$ (Henderson, 1965). Therefore, in this case, we can make use of the fact that the phases of each set of 3-fold related peaks should be the same.

We refined the phase origins for three catalase micrographs which were selected, by minimizing the r.m.s. phase errors, making the assumption that the nearest real values (i.e. 0° or 180°) were correct. The r.m.s. error in single measurements of phase, worked out on this basis, was 39°. On subsequently averaging the symmetry related peaks the r.m.s. error became 28°. A final figure of 25° was then obtained after averaging the data common to all three micrographs. We were thus able to give a reliable phase assignment of 0° or 180° to all of the significant reflections (section (a) above) to a resolution of 9 Å.

Similarly, for three selected purple membrane micrographs, the origins were refined by minimizing the phase differences between symmetry related reflections. The r.m.s. error in single measurements of phase, estimated from the variation between the symmetry related peaks was then 18°. Once the three symmetry related phases were averaged, the standard deviation became 10° to 11°, and finally, less than 10° when phases from all three micrographs were averaged.

These final figures for the phase errors are low, considering that in their calculation we have accorded the strong and the weak peaks equal weight. They correspond to figures of merit (Dickerson *et al.*, 1961) of 0·90 and 0·99, respectively, which are

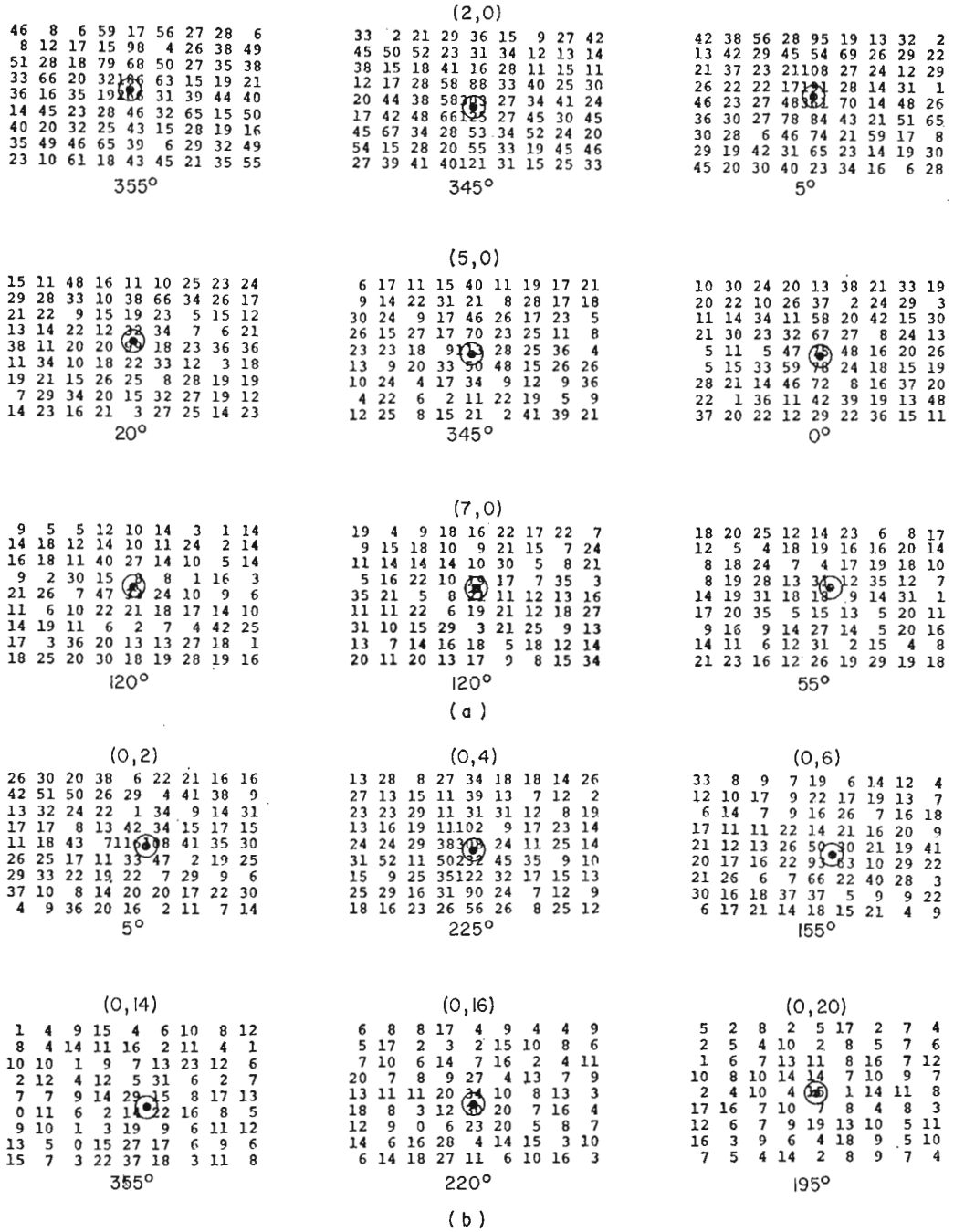

FIG. 3. Fourier transform amplitudes in the region of some typical low and high-resolution peaks, computed from 2048×2048 optical density arrays in (a) a purple membrane micrograph and (b) a catalase micrograph.

The circles identify the calculated positions of each of the peaks (see text), and the phases at these positions are indicated. The strong peaks generally extended over 2 or 3 numbers, in which case they gave almost stationary values for the phase. With some of the weak peaks there were small phase gradients over the calculated positions, but in these cases the phases were able to be interpolated fairly reliably by eye.

higher (particularly in the case of the purple membrane) than those encountered when using the isomorphous replacement method in the X-ray analysis of protein crystals. An additional advantage is that the more important, stronger peaks are phased more accurately. This is not the case with the method of isomorphous replacement,which is often less accurate with stronger reflections.

The projected structures of the catalase crystals and the purple membrane sheets, obtained by Fourier synthesis of the structure factors, as determined above, are shown in Plate VI. The r.m.s. error levels in both structures estimated from the known phase and amplitude errors using the formula of Dickerson *et al.* (1961) are about one contour level.

Since we have already corrected for all imaging phase changes, the positive density regions in the maps correspond to the presence of high-density features in the object. In the case of the purple membrane the high-density matter is the protein ($\rho = 1{\cdot}35$ g/ml) and the low-density matter, the lipid ($\rho = 1{\cdot}00$ g/ml). In the case of the catalase, the mean density of the protein and the glucose fluid do not differ by significant amounts.

5. Discussion

There are several aspects concerning the projections we have just described, which warrant further comment. First, there is the important point that it is the undamaged structures we have determined and *not* radiation-altered versions. The evidence for this is provided in part by the dose-response curves (Fig. 1) which show, by extrapolation to zero dose, that the structure factor amplitudes derived from low-dose diffraction patterns can, at most, be only slightly in error. We can also be sure that the phases in the case of the centrosymmetric catalase projection do not alter during irradiation. Since they can only change by 180°, a change would imply a region of zero intensity in the dose-response curves, which is not observed†. A similar deduction about the accuracy of the phases in the purple membrane case can be made from the almost uniform fading of its diffraction pattern.

The second point to be made is that the projections given in Plate VI correspond to the same distribution of matter one would deduce by X-ray diffraction analysis. They provide information not only on the relatively gross features associated with quaternary structures (as, for example, is the case with conventional images of negatively stained specimens) but on internal detail as well. The projected potential distributions, as we have calculated, are to a good approximation equivalent to the electron density distributions that one would calculate by X-ray methods. Of course, our present structures are not yet at the resolutions we have come to expect from X-ray analysis; the analysis in Results section (c) suggests, however, that they do have the advantage of high accuracy of phase determination.

Our present limitation to resolutions of 7 and 9 Å is caused by the fall-off in contrast transfer of the medium and high spatial frequencies that is evident in the optical diffraction patterns of the images (Plates IV and V; also Fig. 2), although the effect may be influenced somewhat by the presence of non-localised inelastic scattering (Isaacson *et al.*, 1974; Misell & Burge, 1973). The main factor causing this deterioration in contrast transfer is probably some electron optical disturbance (which may be more severe at the magnifications used here than at high magnifications). Other possible

† An exception is the (2, 0) reflection; it however only reappears with doses considerably greater than N', i.e. when all but the very low-resolution reflections have vanished.

contributing factors include the effect of partial coherence (Hanszen & Trepte, 1971; Frank, 1973; Reimer & Gilde, 1973) and spread of the electrons in the photographic emulsion. It can be shown, however, that because of our use of an extremely coherent incident beam and only moderate degrees of under-focus, the effect of partial coherence will be insignificant at ~7 Å resolution. Experiments we have carried out to determine the modulation transfer properties of the photographic plate, indicate that the reduction in contrast due to this source should be no more than 40% at this resolution (for similar results, using 60 kV electrons, see Burge & Garrard (1968)). Anticipating that the major cause of the deterioration will be overcome, it should be possible to solve the projected structures of these specimens to the resolution to which they are preserved (~3·5 Å).

Of the two projections in Plate VI, the catalase projection is the more complex. It can nevertheless be related to the projection obtained by negative staining and interpreted in terms of the superposition of single layers of molecules (Unwin, unpublished results). The possibility that the interpretation of the present projection should include consideration of dynamical interaction (Taylor & Glaeser, 1974) would seem to be discounted by the estimates given earlier. It also seems most unlikely in view of the intensities of some specific reflections in the electron diffraction pattern; the absence of a (0, 8) reflection (which is also absent or very weak in the corresponding X-ray powder pattern), in spite of the presence of a very intense (0, 4) reflection, is for example strong evidence that dynamical effects are unimportant.

The purple membrane, being comprised of a single layer of molecules and having only about one-tenth of the thickness of the catalase crystals, exhibits a minimum degree of superposition in projection and can accordingly be interpreted more directly. The features observed in Plate VI(a) are consistent with an analysis of the X-ray pattern of oriented purple membranes (Henderson, 1975) which showed that the protein in the membrane was composed to a considerable extent of α-helices arranged roughly perpendicular to the plane of the membrane, and which suggested that the lipids were less well-ordered in the lattice, occupying broad contiguous areas between the protein molecules. The high-density peaks, which are 10(±1) Å apart in this projection, are likely to be the helices viewed end-on and in contact with one another, and the broad featureless regions near each of the 3-fold axes, the lipids. We are currently collecting three-dimensional data from the purple membrane by taking micrographs of tilted specimens.

6. Conclusion

It has been demonstrated that one can obtain *in vacuo* preservation of unstained biological specimens to resolutions close to interatomic spacings by replacing their natural aqueous environment with a medium composed of glucose or some similar compound.

Unstained specimens are sensitive to radiation damage. The detail in them can nevertheless be recorded in extremely low-dose, defocussed bright-field electron micrographs.

To determine the structures of the undamaged molecules, periodic arrays containing a redundancy of information and image processing methods are needed. Because of the low inherent contrast and statistically noisy nature of the images, the arrays need to be fairly large (greater than about 1000 unit cells).

Since the resolutions we have currently attained with the projected structures of the purple membrane and of catalase (7 Å and 9 Å, respectively) are not limited by the intrinsic order present (3·5 Å in both), there is a good prospect of obtaining results comparable to those obtained by using the isomorphous replacement method of protein crystallography. The electron microscopy method has the additional advantage of high accuracy of phase determination.

We thank Dr J. Pilkington (Royal Greenwich Observatory) and Dr O. Kübler (Eidg. Technische Hochschule Zurich) for help with the densitometry, Dr U. Aebi and Dr R. Smith (Biozentrum, Universitat Basel) for help with preliminary optical filtering experiments, and Chris Raeburn for construction of equipment for use with the microscope. We are also indebted to our colleagues at this Laboratory and at the Cavendish Laboratory, Cambridge, for valuable discussions and their comments on the manuscript.

REFERENCES

Blaurock, A. E. & Stoeckenius, W. (1971). *Nature (London)*, **233**, 152–154.
Bragg, W. L. & Perutz, M. F. (1952). *Acta Crystallogr.* **5**, 277–283.
Burge, R. E. & Garrard, D. F. (1968). *J. Scient. Instrum.* **1**, 715–722.
Cowley, J. M. & Moodie, A. F. (1957). *Acta Crystallogr.* **10**, 609–619.
Dickerson, R. E., Kendrew, J. C. & Strandberg, B. E. (1961). *Acta Crystallogr.* **14**, 1188–1195.
DeRosier, D. J. & Klug, A. (1968). *Nature (London)*, **217**, 130–134.
Erickson, H. P. & Klug, A. (1970). *Ber. Bunsenges. Phys. Chem.* **74**, 1129–1137.
Erickson, H. P. & Klug, A. (1971). *Phil. Trans. Roy. Soc. ser. B*, **261**, 105–118.
Frank, J. (1973). *Optik*, **38**, 519–536.
Gerchberg, R. W. (1972). *Nature (London)*, **240**, 404–406.
Glaeser, R. M. (1973). *Proc. 31st Annual Meeting EMSA*, (C. J. Arceneaux, Ed.) pp. 226–227, Claitor's Publishing Division, Baton Rouge, U.S.A.
Hamilton, J. F. & Marchant, J. C. (1967). *J. Opt. Soc. Amer.* **57**, 232–239.
Hanszen, K.-J. & Morgenstern, B. (1965). *Z. Ang. Physik.* **21**, 215–227.
Hanszen, K.-J. & Trepte, L. (1971). *Optik*, **33**, 182–198.
Harrison, S. C. (1969). *J. Mol. Biol.* **42**, 457–483.
Henderson, R. (1975). *J. Mol. Biol.* **93**, 123–138.
Hoppe, W. (1970). *Acta Crystallogr. sect. A*, **26**, 414–426.
Huxley, H. E. & Klug, A. (1971). Editors of *New Developments in Electron Microscopy. Phil. Trans. Roy. Soc. ser. B*, vol. 261.
Huxley, H. E. & Zubay, G. (1960). *J. Mol. Biol.* **2**, 10–18.
Isaacson, M., Langmore, J. & Rose, H. (1974). *Proc. 32nd Annual Meeting EMSA*, (C. J. Arceneaux, ed.), pp. 374–375, Claitor's Publishing Division, Baton Rouge, U.S.A.
Matricardi, V. R., Wray, G. & Parsons, D. F. (1972). *Micron*, **3**, 526–539.
McLachlan, D. (1958). *Proc. Nat. Acad. Sci., U.S.A.* **44**, 948–956.
Misell, D. L. & Burge, R. E. (1973). In *Image Processing and Computer-aided Design in Electron Optics* (Hawkes, P. W., ed.), pp. 168–194, Academic Press, New York.
Oesterhelt, D. & Stoeckenius, W. (1974). *Methods in Enzymology*, **31**, 667–678.
Parsons, D. F., Matricardi, V. R., Moretz, R. C. & Turner, J. N. (1974). *Advan. Biol. Med. Phys.* **15**, 162–270.
Reimer, L. & Gilde, H. (1973). In *Image Processing and Computer-aided Design in Electron Optics* (Hawkes, P. W., ed.), pp. 138–167, Academic Press, New York.
Stenn, K. & Bahr, G. R. (1970). *J. Ultrastruct. Res.* **31**, 526–550.
Sumner, J. B. & Dounce, A. L. (1955). *Methods in Enzymology*, **2**, 775–781.
Taylor, K. A. & Glaeser, R. M. (1974). *Science*, **186**, 1036–1037.
Thon, F. (1966). *Z. Naturforsch.* **219**, 476–478.
Thon, F. (1971). In *Electron Microscopy in Materials Science* (Valdrè, U., ed.), pp. 570–625, Academic Press, New York.